Nanoscale tipped microwire arrays enhance electrical trap and depth injection of nanoparticles

Nanoscale tipped microwire arrays enhance electrical trap and depth injection of nanoparticles

Akihiro Goryu[1]**, Rika Numano**[2]**, Akihito Ikedo**[1]**, Makoto Ishida**[1,2] **and Takeshi Kawano**[1]

[1] Department of Electrical and Electronic Information Engineering, Toyohashi University of Technology, Toyohashi, Aichi, Japan
[2] Electronics-Inspired Interdisciplinary Research Institute (EIIRIS), Toyohashi University of Technology, Toyohashi, Aichi, Japan

E-mail: kawano@ee.tut.ac.jp

Abstract
Nanoscale devices have the potential to measure biological tissues as well as individual cells/neurons. However, three-dimensional (3D) multi-site probing remains problematic because only planar-type device designs are applicable to sample surfaces. Herein we report 3D nanoscale electrode tipped microwire arrays with high aspect ratios. A nanoscale tipped wire is formed by isotropic silicon etching to the tip of a vapor–liquid–solid grown silicon microwire. After coating the wire with a metal (e.g., Pt and Au), only the nanotip section can be exposed from the surrounding outer shell (e.g., SiO_2 and parylene) by photoresist spray coating and subsequent cycled photoresist etchings. As a promising device application, we demonstrate the trapping of polystyrene nanoparticles in a solution using a fabricated Au-nanotip wire array. The sharpened nanotip has a 150 nm curvature radius and a 4.2 μm^2 electrode area. The nanotip wires exhibit a locally enhanced trapping performance with a low trapping voltage of 20 mV. Moreover, these trapped nanoparticles can be injected into a soft material (gelatin), demonstrating a multi-site wide-area batch depth injection and an assembly of nanoparticles. Such nanotip wire arrays should be applicable to trap numerous particles, including DNA/molecules attached to Au particles, and may realize injection into biological tissues and individual cells/neurons.

S Online supplementary data available from stacks.iop.org/Nano/23/415301/mmedia

(Some figures may appear in colour only in the online journal)

1. Introduction

Nanoscale devices show great potential as a measurement technology with a high spatial resolution for nanoscale biological experiments [1]. In particular, vertically aligned nanowire devices have enabled numerous biological experiments, including intracellular nanowire penetration, DNA/molecule transfer [2], optical imaging [3], and nanoscale transistor penetration into a cell [4]. To form nanodevices with higher aspect ratios, millimeter length semiconducting nanowires and carbon nanotubes have been synthesized (e.g., silicon nanowires by vapor–liquid–solid (VLS) growth [5] and

carbon nanotubes by a water-assisted synthesis [6]). However, the penetration of such nanowires/tubes deep within a thick biological sample has yet to be demonstrated because nanowires/tubes bend or break with a penetration depth of several tens of microns or the quality degrades upon penetration, preventing the nanowires/tubes from reaching the target tissue or cell.

Thus, an obstacle for nanoscale device applications in biological experiments is deep wire penetration. Deep wire penetration will enable three-dimensional (3D), multi-site, nanoscale measurements in thick biological samples. To realize a penetrating nanodevice array, we have proposed
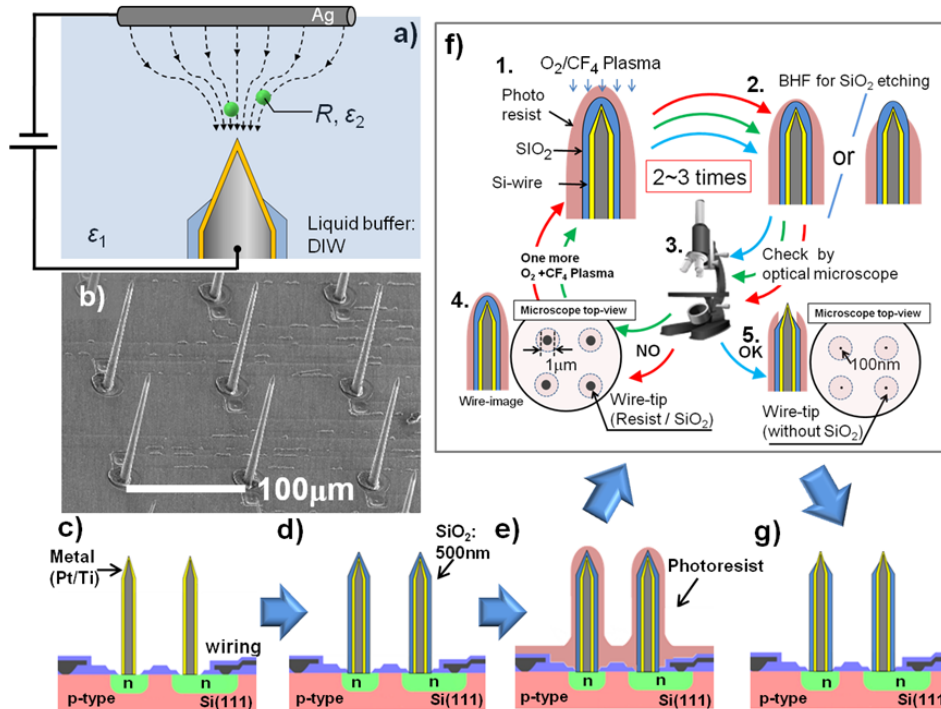
Figure 1. Fabrication of a nanoscale tipped microwire array and its application to a particle trap. (a) Schematic of nanoparticle trapping in a solution by a nanotip electrode where the electrode induces a non-uniform electric field for the DEP force. (b) SEM image of an array of nanotip silicon wires fabricated by VLS growth of silicon microwires and nanotip formation. (c), (d) Nanotip silicon microwires covered with metal (Pt/Ti) and insulating (SiO$_2$) layers. (e) Spray coating of photoresist. (f) Schematics of cycled photoresist and SiO$_2$ etching for nanotip exposure: (1) photoresist etching and (2) SiO$_2$ etching, (3) microscope observation, and (4) top views of nanotips covered with photoresist/SiO$_2$ layers (tip diameter > 1 μm), and (5) nanotips exposed from the photoresist/SiO$_2$ layers (<1 μm). During the cycled etchings, the wire tip diameter observed by the microscope suddenly drops to less than 1 μm once the tip is exposed. (g) Photoresist removal for device compression.

employing a vertically aligned vapor–liquid–solid (VLS) grown silicon microwire scaffold array as a mechanical support [7–9]. In this approach, chemical etching of silicon sharpens the tip section on the nanoscale (<100 nm in diameter at the tip) [10]. The fabrication process developed in this paper facilitates nanoscale electrode tipped microwire array devices, and the results suggest that the nanowire array has applications for both particle trapping and particle depth injections. Advantages of the fabrication process include low-voltage electrical trapping over a wide area and batch particle manipulation with a constant wire interval.

Figure 1(a) schematically illustrates the electrical particle trapping mechanism. Trapping is demonstrated using polystyrene nanoparticles in deionized water (DIW), where the particle trapping force is based on the electric field induced by the nanotip electrode with a bias voltage, which can be explained by the direct current dielectrophoresis (DC-DEP) force [11–13], and is expressed as

$$\bar{F}_{\mathrm{DEP}} = 2\pi\varepsilon_1 R^3 \left(\frac{\varepsilon_2 - \varepsilon_1}{\varepsilon_2 + 2\varepsilon_1}\right)\nabla E^2 \qquad (1)$$

where ε_1 is the fluid of dielectric permittivity (DIW). ε_2 and R are the dielectric permittivity and the radius of a dielectric sphere (polystyrene nanoparticle), respectively. E is a non-uniform electric field. The trapping force in DEP is proportional to ∇E^2; a sharpened nanotip electrode with

a small surface area increases the electric field [14]. The proposed fabrication process can realize such a sharpened nanotip electrode.

2. Fabrication of nanotip wire arrays

The integration and 3D fabrication techniques proposed here can realize vertical microwire arrays with a nanotip electrode and a high aspect ratio. Figure 1 shows the sequence of techniques to prepare a nanotip silicon microwire array using VLS growth and nanotip formation [10]. Fabrication details for the IC-processed interconnections prior to the VLS growth appear in the supporting information (SI) (available at stacks. iop.org/Nano/23/415301/mmedia). Herein we use ∼120 μm long and 2 μm diameter n-type silicon wires with a resistivity of 10^{18} cm^{-3}, which are synthesized by Au-catalyzed VLS growth with a mixed gas containing 1% PH$_3$ (diluted in 99% hydrogen) with 100% Si$_2$H$_6$ at a gas pressure of 0.6 Pa and a growth temperature of 700 °C [15]. After fabricating the nanotip silicon microwire array (50 nm curvature radius) (see SI available at stacks.iop.org/Nano/23/415301/mmedia), the entire wire array is metallized. Herein a 30 nm platinum (Pt) with an adhesion layer of 20 nm titanium (Ti) is coated by sputtering (figure 1(c)), yielding a Pt nanotip with a 70 nm curvature radius (see figure SI 2(b) and (c) available at stacks. iop.org/Nano/23/415301/mmedia). The insulating layer, SiO$_2$
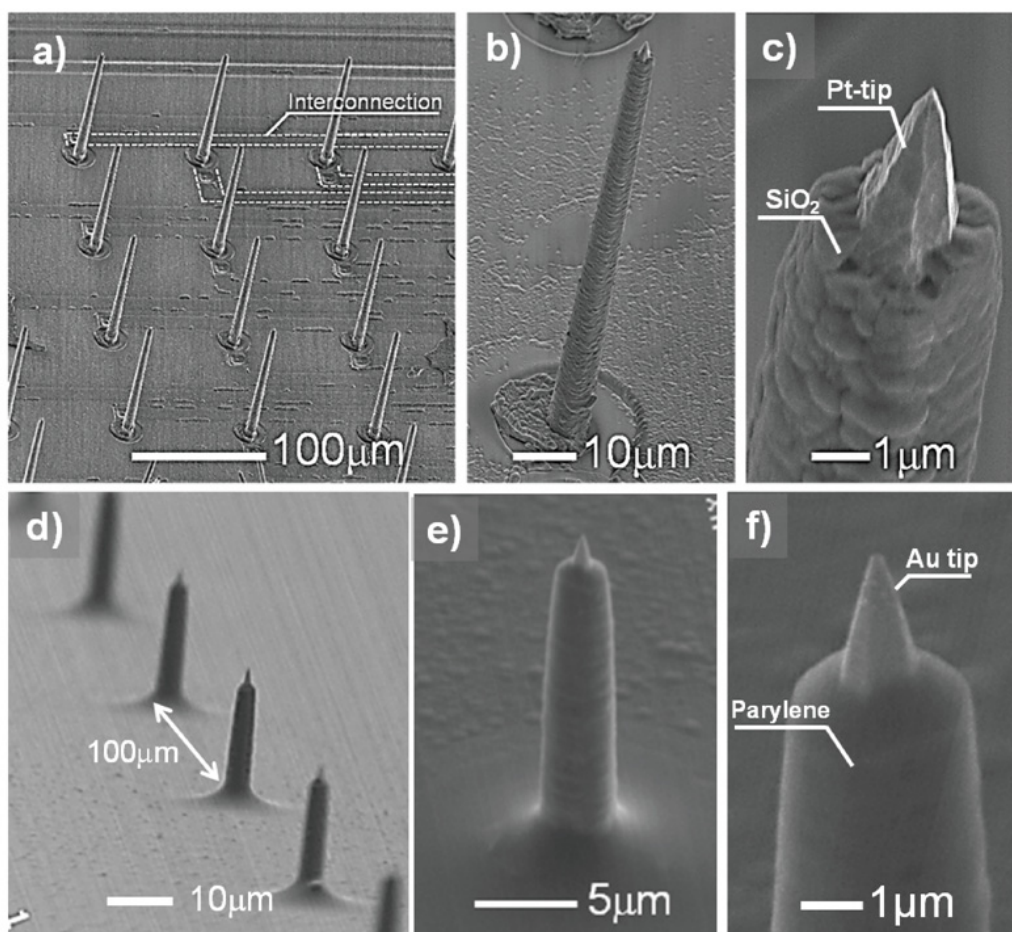
Figure 2. SEM images of the fabricated nanotip microwire arrays. (a) 3×4 array of Pt-nanotip microwires with a wire height of 120 μm, (b) an individual wire in the same array, and (c) tip section of the same wire showing the exposed Pt-nanotip electrode from the SiO$_2$ shell with an exposed height of 2 μm. (d) Array of Au-nanotip microwires with a wire height of 20 μm, (e) individual wire in the same array, and (f) tip section of the same wire showing an exposed Au-nanotip electrode with a height of 2 μm from the parylene shell.

(500 nm), is formed by plasma chemical vapor deposition (CVD) (figure 1(d)).

To expose the tip, the entire wire is first covered with a photoresist layer (AZ-5218E, viscosity 40cP, $\sim$3 μm thick for planar samples) by spray coating (USHIO, USC-2000ST) (figure 1(e)). Then plasma etchings by O$_2$/CF$_4$ plasma remove the photoresist at the nanotip section with a nano/microscale thickness. A buffered hydrofluoric acid solution (BHF) is used for the subsequent SiO$_2$-etching. With 'cycled' photoresist and SiO$_2$ etchings (see the nanotip patterning section), a Pt nanotip with a nano/microscale height can be exposed from the photoresist/SiO$_2$ shell (figure 1(f)). Finally, the photoresist is removed, and the device is complete.

3. Nanotip patterning techniques

To expose the Pt nanotip from the SiO$_2$ shell of the vertical microwire, cycled etching-based photoresist patterning is used (figure 1(f)). After spray coating the photoresist over the wire (figure 1(e)), we conducted the photoresist etching with O$_2$/CF$_4$ plasma (figure 1(f)(1)) and subsequent underneath SiO$_2$ etching with BHF (figure 1(f)(2)). Although the length

of photoresist etching is insufficient to expose the Pt nanotip from the SiO$_2$ shell, microscopy confirmed the shape of the photoresist and a diameter greater than 1 μm (figures 1(f)(3–4)). These observations indicate that repeating the process (photoresist etching and SiO$_2$ etching) is necessary until the exposed Pt nanotip has a confirmed diameter less than 1 μm (figure 1(f)(5)). For the O$_2$/CF$_4$ plasma etching, herein we used a gas pressure of 53 kPa (O$_2$: 40 sccm, CF$_4$: 5 sccm), yielding a photoresist etching rate of 1 μm min^{-1}; this rate allows sub-micron scale control of the photoresist.

With this methodology, the Pt-nanotip section with a microscale height is exposed from the photoresist/SiO$_2$ shell (figures 2(a)–(c)). Figure 2(b) is a wire in the array with a controlled exposed height of 2 μm (figure 2(c)). Cycled etchings of the photoresist/SiO$_2$ are repeated three times, where the first, second, third cycles last 60 s, 60 s, and 30 s, respectively. Each subsequent SiO$_2$ etching time is 1 min. Although the exact thickness of the photoresist over the tip section is unknown after spray coating (figure 1(e)), the proposed cycled etching process can be used for controlled batch exposure of the nanotips from SiO$_2$ shells.

Based on the parameters of the photoresist coating and the cycled etching, we then prepared 20 μm long
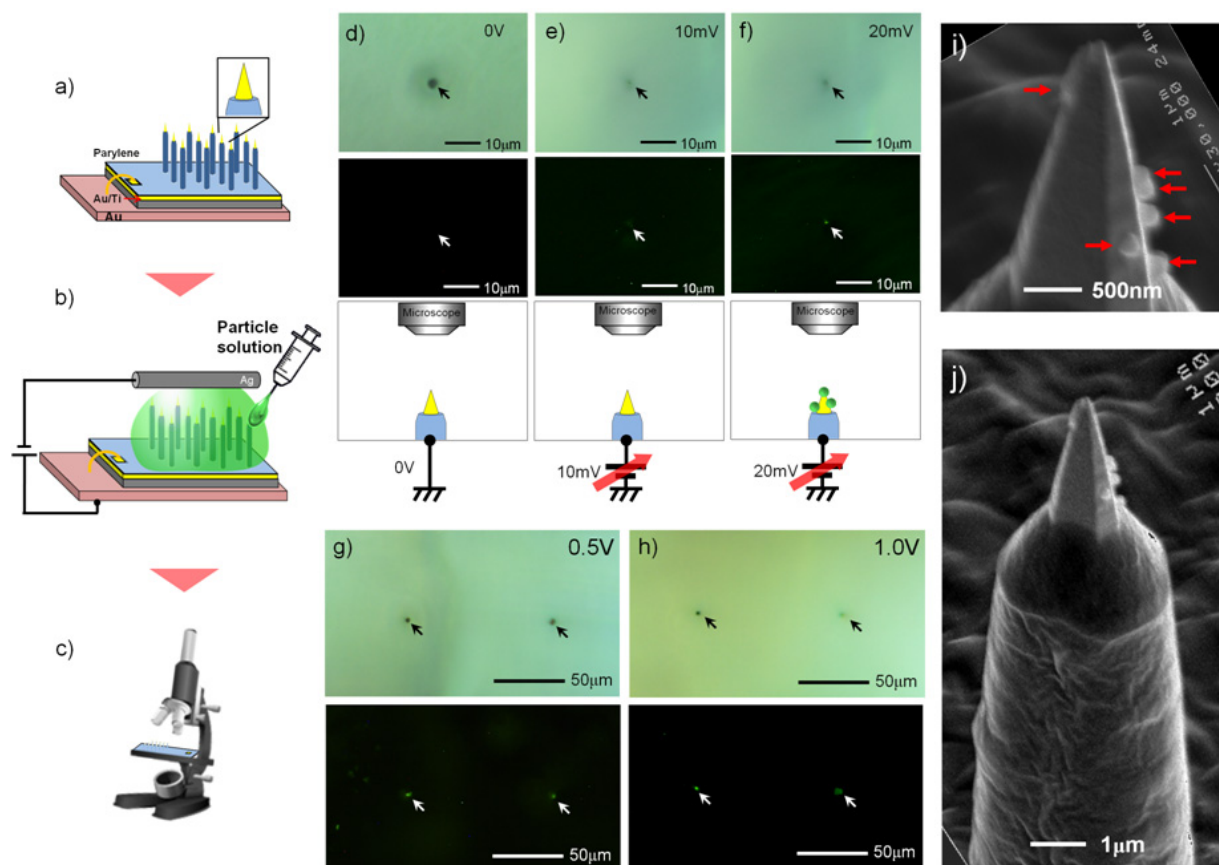
Figure 3. Electrical trapping of nanoparticles via a Au-nanotip wire array. Schematic images of the device and trapping steps: (a) packaged Au-nanotip array with an external metal wire (Au) to apply device biases, (b) electrical trapping of nanoparticles in a nanoparticle solution with a device bias, and (c) fluorescence observation of trapped nanoparticles. (d)–(f) Brightfield (top), fluorescence (middle), and schematic (bottom) images of a nanotip wire after particle trapping with bias voltages of 0 V, 10 mV, and 20 mV, respectively. (g)–(h) Brightfield (top) and fluorescence (bottom) images of two Au-nanotip wires after trapping with bias voltages of 0.5 V and 1.0 V, respectively. (i) Close-up and (j) overall SEM images of a nanotip section after particle trapping with a bias voltage of 1.0 V. Red arrows in the image (i) mark nanoparticles.

Au-nanotip microwire arrays because Au has the potential to effectively trap DNA and other molecules; in the future, we plan to report an application for DNA/molecule injection into a biological sample. The Au-nanotip microwire array is prepared using a fabrication process similar to that for Pt-nanotip microwires (figure 1), except the insulating shell of parylene-C with the biocompatible property differs. After fabricating a silicon-nanotip microwire, the wire is metallized with a 100 nm Au/20 nm Ti adhesion layer by sputtering (figure 1(c)), resulting in a Au nanotip with a 150 nm curvature radius. The wire is subsequently encapsulated with ∼800 nm parylene. The exposed height of the Au nanotip is 2 μm (figures 2(d)–(f)), which can be controlled by the parameters of the cycled etching. The exposed Au surface area of a nanotip wire is 4.2 μm^2.

4. Nanoparticle trap

To demonstrate electrical trapping of particles using polystyrene nanoparticles in DIW, herein we use an array of 20 × 20 Au-nanotip microwires (figures 2(d)–(f)). Each Au nanotip is electrically connected to a common Au wire

to achieve batch nanoparticle trapping (figure 3(a)). The Au wire is covered with insulating silicone for particle trapping in an aqueous environment. Figures 3(b) and (c) illustrate the essential steps for nanoparticle trapping: electrical trapping of nanoparticles and sample observation after rinsing particles except for the trapped particles. A droplet (10 μl) of DIW, which consists of fluorescent polystyrene nanoparticles (Merck F1-XC010, modified with COOH, excitation wavelength = 485 nm, fluorescence emission wavelength = 510 nm, nanoparticle diameter = 167 nm ± 9 nm), is placed on a positively biased device using a micropipette (figure 3(b)). Next, electrically trapped particles are transferred to a DIW solution bath to remove excess particles. After rinsing, fluorescence microscopy (Olympus BX51, Olympus, Japan) is used to confirm the trapped nanoparticles (figure 3(c)).

Electrical trapping of nanoparticles via Au-nanotip electrodes is clearly observed upon applying a device bias voltage. Figures 3(d)–(f) show the result of nanoparticle trapping; the top and middle images are the brightfield and fluorescence microscope images of the tip section of the Au nanotip, respectively. Particle traps do not occur at the

tip section without an electrical device bias (figure 3(d)). Increasing the device bias to 10 mV does not induce nanoparticle traps (figure 3(e)). However, all Au-nanotip sections with a device bias of 20 mV clearly display nanoparticle traps (figure 3(f)). These experimental results suggest that 20 mV is the threshold bias of the particle trap in this scheme. As the device bias is further increased, the trapped nanoparticles become saturated. Figures 3(g) and (h) show particle traps at device biases of 0.5 V and 1.0 V, respectively, and their fluorescence images do not significantly differ. We also quantitatively investigated the number of nanoparticles trapped at the nanotip sections by acquiring SEM pictures after trapping the particles. Figures 3(i) and (j) (and SI3 available at stacks.iop.org/Nano/23/415301/mmedia) show a maximum of six nanoparticles trapped at a bias voltage of 1.0 V, which represents observations on one side of the tip section. In addition, the change in the particle shape is insignificant (figures 3(i) and (j)) and the particles are not damaged on any of the 15 nanotip wire samples (Figure SI3 available at stacks.iop.org/Nano/23/415301/mmedia). It should be noted that electrolysis of a solution at the Au-nanotip section occurs when the device bias exceeded 2.0 V.

The aforementioned formula (1) indicates that the particle trapping force is proportional to ∇E^2. Thus, we employed finite element method analysis (ANSYS, Ansys Inc., Canonsburg, USA) [14] to calculate the electric field distributions in DIW while applying a device bias to a Au-nanotip wire (simulated parameters: tip curvature radius = 150 nm; permittivity of DIW = 80; and resistivity of DIW = $10 \times 10^6 \, \Omega$ cm). The calculated maximum electric field at the tip section of the wire is 6.19×10^3 V m^{-1} with an applied threshold device bias of $+20$ mV (see figure SI4a available at stacks.iop.org/Nano/23/415301/mmedia). The maximum electric field of the nanotip wire is approximately twice that of a 2 μm diameter hemispherical tipped microwire (3.11×10^3 V m^{-1}) whose shape is consistent with the wire tip before nanotip formation (see figure SI4b available at stacks.iop.org/Nano/23/415301/mmedia). Moreover, the simulation results also indicate decreasing the tip angle and/or the curvature radius of the wire tip can further enhance the electric field. Nanotip formation with a HF–HNO$_3$ solution provides tip angle control, which is a parameter of efficiency for an electric field-based particle trap; we have demonstrated that the tip angle can be controlled between 11° and 38° [10]. A slower silicon-etching rate (<0.6 μm min^{-1}) can decrease the tip angle, while an additional process of cycled thermal oxidation of the silicon nanotip and the oxide removal can produce a smaller curvature radius of the tip (<150 nm) [16]. Moreover, HF–HNO$_3$ solution-based silicon etching provides roughness control for an etched silicon surface [17]. Roughness is the other considerable parameter for electric field-based trapping efficiency. Due to the surface-area-dependent electric field, decreasing the exposed electrode surface area (<4.2 μm^2) may realize a higher electric field ($>6.19 \times 10^3$ V m^{-1}) [14]. Hence, cycled photoresist patterning with a shorter photoresist etching time (<30 s) may reduce the exposed electrode surface area (figure 1(f)(1)–(2)).

5. Nanoparticle injection

Trapped nanoparticles can be injected into a soft material such as gelatin. Figures 4(a)–(c) illustrate the steps of a batch nanoparticle injection into a gelatin (6.7 wt% in water) in a 'stamp' usage. Herein nanoparticles are trapped at 1.0 V device bias prior to injection (figure 3). It should be noted that the same device bias (1.0 V) is applied during wire penetration, but a device bias is not applied during wire extraction (see SI text and figure SI5 available at stacks.iop.org/Nano/23/415301/mmedia). We also assessed device damage due to the procedures involved in particle trapping and gelatin injection. SEM images (figure SI6 available at stacks.iop.org/Nano/23/415301/mmedia) of the nanotips after wire extraction from the gelatin do not exhibit breakage and/or damage, indicating that the nanotips have sufficient robustness as particle traps and gelatin injectors. Additionally, these SEM observations indicate that particles remain at the nanotip after one session of gelatin injection. One reason some particles remain is that pieces of gelatin surround the nanotip surface, contributing an additional holding force between the particle and the nanotip surface.

Figure 4(d) is a top-view of the florescence microscope image of the gelatin after particle injection, and shows that nanoparticles are injected and assembled in the gelatin. A confocal microscope (Zeiss LSM 700, Zeiss, Germany with 488 nm excitation and 510 nm fluorescence emission) is used to analyze the depth (Z axis) position of the nanoparticles in the gelatin. The fluorescence intensities indicate the gaps between particle clusters are spaced approximately 100 μm apart (figure 4(f), Olympus BX51, Olympus, Japan), which is the same as that of the nanotip microwire array (100 μm site spacing). Nanoparticles in the gelatin appear as green signals in figure 4(h), indicating that the nanoparticles can be placed using a nanotip wire array in various locations from the surface of the gelatin up to a depth of 20 μm, which is consistent with the height of the nanotip wire.

One effect of releasing particles from the Au nanotip is the adhesion force between the particle and the gelatin. The adhesion force between the particle and the gelatin is higher than that between the particle and Au electrode. The adhesion force between the Au nanotip and a nanoparticle can be discussed with the Derjaguin approximation [18, 19],

$$F_{\text{Au}-\text{Par}} = 4\pi \left(\frac{R_{\text{Au}} R_{\text{Par}}}{R_{\text{Au}} + R_{\text{Par}}} \right) \gamma_{\text{Au}-\text{Par}} \qquad (2)$$

where R_{Par} is the radius of a nanoparticle, and R_{Au} is the curvature radius of the area in the Au electrode where the nanoparticle is trapped (see figure SI7 available at stacks.iop.org/Nano/23/415301/mmedia). $\gamma_{\text{Au}-\text{Par}}$ is the surface energy per unit area of the Au/particle interface, and $F_{\text{Au}-\text{Par}}$ is the adhesion force between the Au-nanotip area and the particle. Due to the trapping bias of 1.0 V ($>$threshold bias of 20 mV), the number of particles trapped in area varies considerably from the end to the base of the exposed Au electrode ('R_{Au}' represents these varied curvature radii, as shown in figure SI7 available at stacks.iop.org/Nano/23/415301/mmedia). Assuming a large curvature radius for
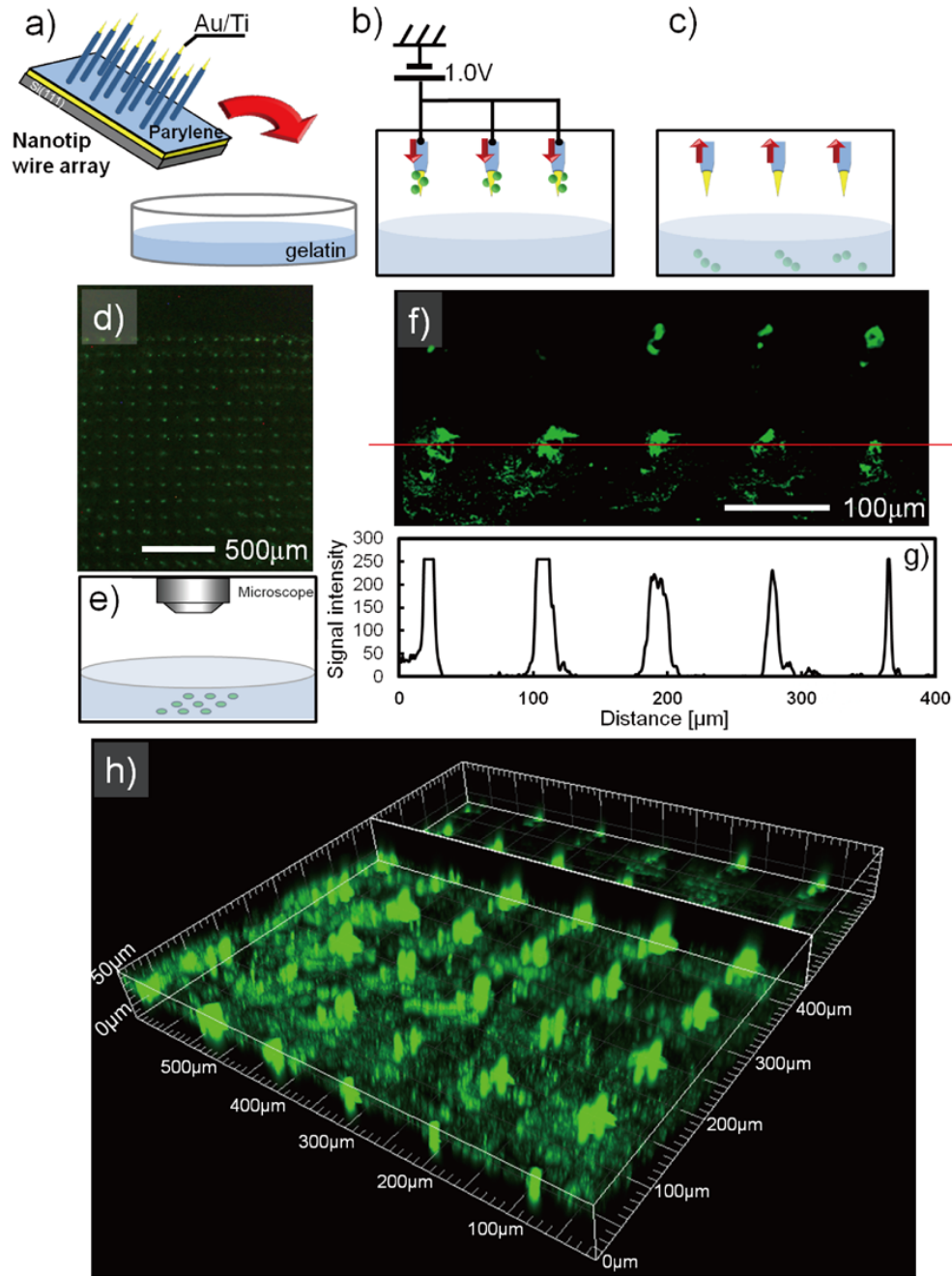
Figure 4. Deep nanoparticle injection along a wide area into a gelatin. (a)–(c) Schematic images of the injection steps. Prior to injection, nanoparticles are trapped in the particle solution by applying a device bias of 1.0 V (figures 3(h)–(j)). (a) Au-nanotip array with trapped particles penetrates into a gelatin in a 'stamp' usage. (b) A device bias of 1 V is employed during the gelatin penetration, and (c) no electrical bias is applied during the extraction from gelatin. (d) Top-view image of gelatin after nanoparticle injection, and (e) schematic image of a particle injected into gelatin. (f) Top-view image of the confocal microscope observation of the gelatin. (g) The particle emitting intensity distance curve taken from the image in (f). (h) 3D particle distribution in gelatin. Note that the bottom of the image is consistent with the surface of the gelatin (injected side).

R_{Gel} compared to that of the nanoparticle ($R_{Gel.} \gg R_{Par.}$), the adhesion force between the nanoparticle and the gelatin becomes

$$F_{Par-Gel} = 4\pi R_{Par}\gamma_{Par-Gel} \qquad (3)$$

where $\gamma_{Par.-Gel}$ is the surface energy per unit area of the nanoparticle/gelatin interface and $F_{Par-Gel}$ is the adhesion force between the nanoparticle and gelatin. Herein the

adhesion force ratio of $F_{Par-Gel}/F_{Au-Par}$ exceeds one, which is demonstrated by the injections where the nanoparticles are released from the Au nanotip to the gelatin,

$$\frac{F_{Par-Gel}}{F_{Au-Par}} = \left(1 + \frac{R_p}{R_{Au}}\right)\frac{\gamma_{Par-Gel}}{\gamma_{Au-Par}} > 1. \qquad (4)$$

Although the surface energies of γ_{Au-Par} and $\gamma_{Par-Gel}$ are not quantitatively known, the ratio of $F_{Par-Gel}/F_{Au-Par}$ indicates

that the adhesion force ratio can be increased by decreasing the curvature radius for R_{Au}. As previously mentioned, by decreasing the tip angle and/or reducing the tip curvature radius, such Au nanotips can enhance the performance of the adhesion force-based nanoparticle release. In addition, Au nanotips with a small curvature radius play important roles in the trapping efficiency of an electric field-based nanoparticle trap. Moreover, this device takes advantage of the injection capability for numerous molecules and markers, which can be placed deeply and selectively in biological samples, such as brain tissue, because a sharpened Au nanotip is minimally invasive to living cells and has high trapping and releasing efficiencies.

6. Conclusion

In summary, we propose localized trapping of nanoparticles using a nanoscale electrode tipped microwire array with a low device bias. Employing a sharpened nanotip electrode with a small surface area can enhance the electric field-dependent trapping force. Such nanotip microwire array devices can be fabricated by spray coating the photoresist and cycled photoresist etchings. Although herein we demonstrate the particle trap and injection capabilities of a nanotip array using polystyrene nanoparticles, numerous other particles can be successfully trapped and injected, making these microwire arrays powerful for applications to 3D nanoparticle assemblies in soft materials.

Acknowledgments

References

[1] Patolsky F, Timko B P, Yu G, Fang Y, Greytak A B, Zheng G and Lieber C M 2006 *Science* **313** 1100–4
[2] Singhal R, Orynbayeva Z, Sundaram R V K, Bhattacharyya S, Vitol E, Niu J J, Schrlau M, Papazoglu E, Friedman G and Gogotsi Y 2011 *Nature Nanotechnol.* **6** 57–64
[3] Xie C, Lindsey H, Cui Y and Cui B 2011 *Proc. Natl Acad. Sci.* **108** 3894–9
[4] Tian B, Cohen-Karni T, Qing Q, Duan X, Xie P and Lieber C M 2010 *Science* **329** 831–4
[5] Wagner R S and Ellis W C 1964 *Appl. Phys. Lett.* **4** 89–90
[6] Hata K, Futaba D N, Mizuno K, Namai T, Yumura M and Iijima S 2004 *Science* **306** 1362–5
[7] Kawano T, Kato T, Tani R, Takao H, Sawada K and Ishida M 2004 *IEEE Trans. Electron Devices* **51** 415–20
[8] Kawano T, Harimoto T, Ishihara A, Takei K, Kawashima T, Usui S and Ishida M 2010 *Biosens. Bioelectron.* **25** 1809–15
[9] Okugawa A, Mayumi K, Ikedo A, Ishida M and Kawano T 2011 *IEEE Electron Device Lett.* **32** 683–5
[10] Goryu A, Ikedo A, Ishida M and Kawano T 2010 *Nanotechnology* **21** 125302
[11] Kang K H, Xuan X, Kang Y and Li D 2006 *J. Appl. Phys.* **99** 064702
[12] Kang Y, Li D, Kalams S A and Eid J E 2008 *Biomed. Microdevices* **10** 243–9
[13] Jones T B 1995 *Electromechanics of Particles* (Cambridge: Cambridge University Press)
[14] Mcintyre C C and Grill W M 2001 *Ann. Biomed. Eng.* **29** 227–35
[15] Ikedo A, Ishida M and Kawano T 2011 *J. Micromech. Microeng.* **21** 035007
[16] Marcus T B, Ravi T S, Gmitter T, Chin K, Liu D, Orvis W J, Ciarlo D R, Hunt D E and Trujillo J 1990 *Appl. Phys. Lett.* **56** 236–8
[17] Schwarts B and Robbins H 1976 *J. Electrochem. Soc.* **123** 1903–9
[18] Junno T, Deppert K, Montelius L and Samuelson L 1995 *Appl. Phys. Lett.* **66** 3627–9
[19] Israelachvili J N 1991 *Intermolecular and Surface Forces* (New York: Academic)